

Combinatorial split-ring and spiral meta-resonator for efficient magnon-photon coupling

Yuzan Xiong,¹ Andrew Christy,^{1,2} Yun Dong,¹ Andrew H. Comstock,³ Dali Sun,³ Yi Li,⁴ James F. Cahoon,² Binbin Yang,^{5, a)} and Wei Zhang^{1, b)}

¹⁾ *Department of Physics and Astronomy, University of North Carolina at Chapel Hill, Chapel Hill, NC 27599, USA*

²⁾ *Department of Chemistry, University of North Carolina at Chapel Hill, Chapel Hill, NC 27599, USA*

³⁾ *Department of Physics and Organic and Carbon Electronics Lab (ORaCEL), North Carolina State University, Raleigh, NC 27695, USA*

⁴⁾ *Materials Science Division, Argonne National Laboratory, Argonne, IL 60439, USA*

⁵⁾ *Department of Electrical and Computer Engineering North Carolina A&T State University, Greensboro, NC 27411, USA*

(Dated: 18 March 2024)

Developing hybrid materials and structures for electromagnetic wave engineering has been a promising route towards novel functionalities and tunabilities in many modern applications. Despite its established success in engineering optical light and terahertz waves, the implementation of meta-resonators operating at the microwave band is still emerging, especially those that allow for on-chip integration and size miniaturization, which has turned out crucial to developing hybrid quantum systems at the microwave band. In this work, we present a microwave meta-resonator consisting of split-ring and spiral resonators, and implement it to the investigation of photon-magnon coupling for hybrid magnonic applications. We observe broadened bandwidth to the split ring modes augmented by the additional spiral resonator, and, by coupling the modes to a magnetic sample, the resultant photon-magnon coupling can be significantly enhanced to more than ten-fold. Our work suggests that combinatorial, hybrid microwave resonators may be a promising approach towards future development and implementation of photon-magnon coupling in hybrid magnonic systems.

I. INTRODUCTION

The emerging needs for quantum technologies require information propagation over long distances and with preserved coherence. This can be achieved by developing hybrid systems consisting of two subsystems operating in a strong-coupling regime^{1–6}. For this purpose, microwave resonators loaded by a low-damping ferrimagnet, e.g., $\text{Y}_3\text{Fe}_5\text{O}_{12}$ (YIG), implementing the strong photon-magnon coupling are often used⁷. Coherent transfer of information can be subsequently achieved between electromagnetic (EM) carrier to various other excitations, such as spin oscillations, acoustic phonons, and qubits^{8–14}.

Among various strategies for improving the photon-magnon coupling strength, engineering the microwave (MW) photon mode, whether in 3-D cavities¹⁵, planar resonators^{16–18}, or cryogenic platforms^{19–22}, remains an effective approach for realizing strongly coupled systems, as the coupling strength is directly proportional to geometrical considerations such as the filling factor of the magnon counterpart by the magnetic component, h , of the resonator EM field²³. In particular, the design of a split-ring resonator (SRR) and its derivatives have been widely adopted in numerous photon-magnon systems,

due to the various advantages including but not limited to subwavelength operation, negative permittivity and permeability, and broadband circuit integration^{24–28}.

In general EM wave engineering, using hybrid structures allows strong localization and field enhancement which enable important novel functionalities with improved compatibility for various applications²⁹. The EM properties can be controlled by tailoring the geometric dimension and metallic structure, whose enlarged design parameter space allows to access and improve characteristics of the bandwidth, frequency selectivity, polarization and size miniaturization. Besides, by further confining the EM fields at the surface through localized modes, surface plasmonic meta-resonators are particularly promising for applications that require ultra-strong matter-field interactions in the near-fields^{30,31}. In this regard, great success of using meta-resonators has been demonstrated primarily in the terahertz (THz) EM engineering^{32,33}, however, still remains elusive for the photon-magnon systems in the MW band.

In this work, we present a combinatorial double-split-ring resonator (DSRR) incorporating a spiral-shaped, meta-resonator for hybrid magnonic applications. Compared to the single split-ring that has been dominantly used, the use of a double-split-ring spectrally extends the bandwidth to a lower frequency region, and more importantly, spatially re-distribute the magnetic field (h -component) towards the center of the resonator³⁴. The latter is particularly important for additional metallic constructions inside the center dielectric area. On the

^{a)}byang1@ncat.edu

^{b)}zhwei@unc.edu

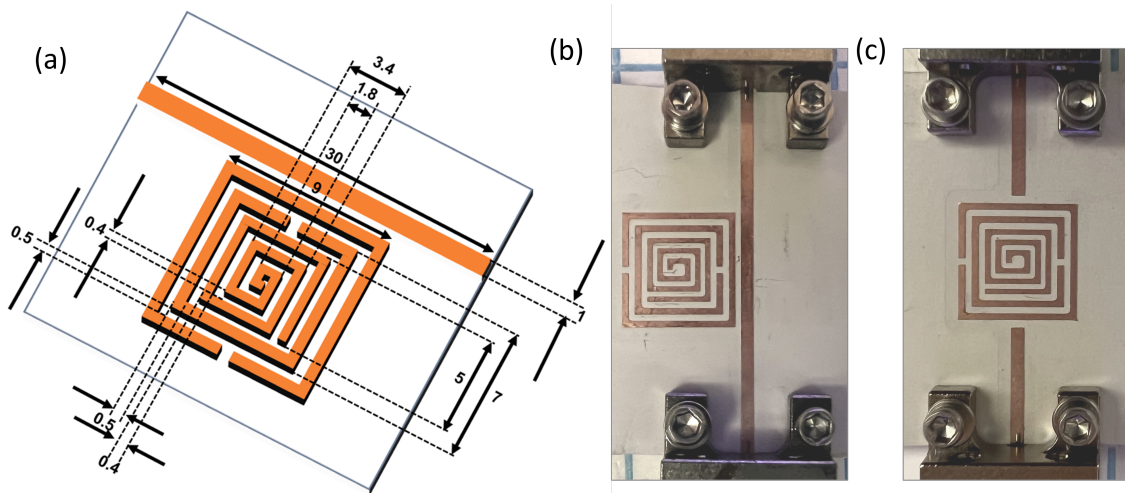


FIG. 1. (a) Schematic illustration and dimensional specification of the s-DSRR meta-resonator. Unit is in mm. The meta-resonator is implemented to either (b) the transmission-line coupled (inductive) or (c) the edge-coupled (capacitive) MW feeding mechanism.

other hand, the spiral resonator has been frequently implemented in miniaturized and multi-resonant MW circuit applications such as wireless sensing, selective filters, and chipless RFID Tags^{35–38}. However, a generic spiral resonator does not couple effectively to an adjacent stripline and the amplitude usually decays rather rapidly as the distance to the MW transmission line increases.

Here, we incorporate a spiral resonator in the center of the DSRR and construct a metamaterial MW resonator with structural symmetry breaking, termed as spiral(s)-DSRR, leveraging its multi-resonance characteristics and an enhanced magnetic coupling (to magnetic samples) due to the increased filling factor and the formation of localized, trapped microwave modes^{39–41}.

We study the spatial properties of the electric- and magnetic-field distribution of the meta-resonator and investigate its application in the context of strong photon-magnon coupling with magnetic YIG samples. We show that additional MW photon modes emerge by adding a spiral resonator to the generic DSRR, and the resultant photon-magnon coupling can be significantly enhanced to more than ten-fold. The results are further corroborated by using microwave simulations. Our design of a combinatorial DSRR and spiral resonator may be treated as a general design protocol for the unit-cell of MW metamaterial future construction of photon-magnon coupled systems.

II. EXPERIMENT AND RESULTS

A. Design and photon resonances of s-DSRR

Figure 1(a) illustrates our key design of the combinatorial s-DSRR. The outer ring of the DSRR has a dimension of $9 \times 9 \text{ mm}^2$, with a conductor width $w = 0.5 \text{ mm}$. The inner ring has a dimension of $7 \times 7 \text{ mm}^2$, and is placed

at a distance of 0.5 mm from the outer ring. The split portion of the inner ring has a width of 0.5 mm. The meta-resonator consists of the DSRR with the same dimension mentioned above and an additional spiral loop in the middle of the resonator dielectric region. The distance of the spiral to the inner ring of the DSRR is 0.4 mm.

We implement the meta-resonator to either a transmission-line, Fig. 1(b), or an edge-coupled microstrip, Fig. 1(c). In the former, the distance between the outer ring to the feeding transmission line, which is 1 mm wide, is 0.45 mm. In the latter, the gap between the microstrip and the outer ring is 0.6 mm. All resonators and the microstrips (transmission or edge-coupled) that feeds them were fabricated on the Rogers TMM Laminates dielectric substrate (Rogers Corp.) with dielectric properties (ϵ_r) of 9.8, tangent loss ($\tan\delta$) of 0.0020, substrate thickness of $T_s = 1.27 \text{ mm}$, and a copper layer thickness of $T_{Cu} = 35 \mu\text{m}$.

The split-ring structure introduces the inductive and capacitive responses to the time-varying electric and magnetic fields from the transmission line or the microstrip. The use of DSRR spatially re-distributes the magnetic field (h -component) towards the center of the resonator (in the dielectric) and with higher uniformity, as opposed to localize on the resonator side near the gap to the MW feed. The spiral loop inside the DSRR is then introduced in the middle. Such a combination enhances the magnetic coupling between the magnetic sample and the subwavelength-based meta-resonator structure, and gives rise to improved polarization characteristic which further enhances the negative electric and magnetic susceptibility. The metallic layer of copper exhibits the inductive response, whereas the dielectric substrate and the space between the metallic arms, are responsible for the capacitive response. For the edge-coupled stripline in Fig. 1(c), the gap between the feedline and the resonator

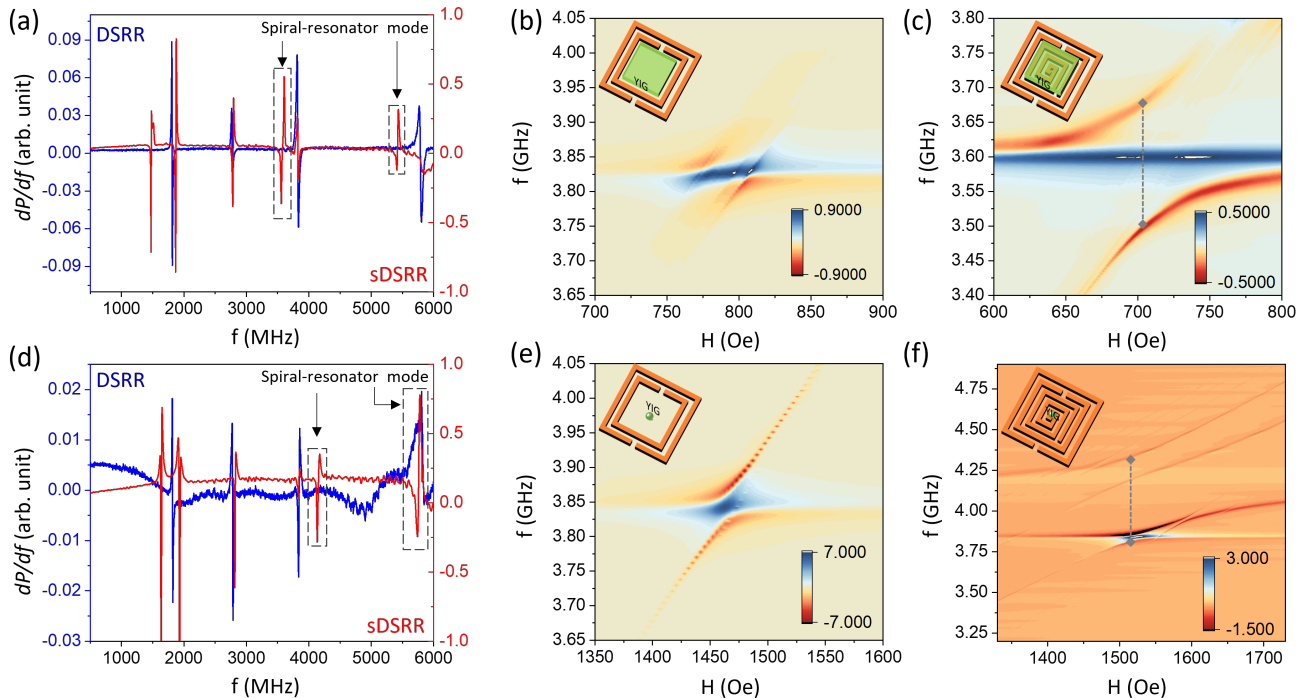


FIG. 2. Results for the transmission-line coupled (inductive) resonator: (a) Absorption spectrum dP/df of the DSRR and s-DSRR when a YIG planar film is loaded. Additional peaks emerge for the s-DSRR compared to the generic DSRR. 2D contour plot of the $[f, H]$ -dispersion showing the photon-magnon coupling: (b) with the DSRR photon mode at 3.83 GHz, and (c) with the s-DSRR photon mode at 3.58 GHz. (d) Absorption spectrum dP/df of the DSRR and s-DSRR when a YIG sphere is loaded. 2D contour plot of the $[f, H]$ -dispersion showing the photon-magnon coupling: (e) with the DSRR photon mode at 3.85 GHz, and (f) with the s-DSRR photon mode at 4.16 GHz.

acts as a parallel plate with additional capacitance to further enhance the quality(Q)-factor but at a cost of higher insertion loss⁴². Inside the s-DSRR region, the inductive properties of the metallic layer dominate over the capacitive value of dielectric substrate, which is the key to an enhanced photon-magnon coupling.

B. Photon-magnon coupling of s-DSRR

We first focus on the meta-resonator coupled to the transmission line, Fig. 1(b), and compare the spectra characteristics of the s-DSRR and the pristine DSRR, measured by using a vector-network analyzer (VNA) up to 6 GHz with the application of an external magnetic field, H , perpendicular to the transmission line, to satisfy the ferromagnetic resonance condition. The resonance peaks (photon modes) are more clearly identified by the derivative absorption dP/df than the conventional S_{21} .

We investigate the photon-magnon coupling of our s-DSRR to magnetic YIG samples. Both planar YIG film (cut into the size of the spiral resonator) and YIG spheres are used. The thickness of the YIG film is 2.0 μm on a 0.5 mm thick gadolinium gallium garnet (GGG) substrate. The nominal diameter of the YIG sphere is 1.0 mm. After loading the YIG sample (either the planar film or the

sphere), slight shifts of the photon modes can be observed due to the change of impedance. In addition, new modes emerge which are unique to the s-DSRR compared to the original DSRR. Figure 2(a) summarizes the absorption spectra (dP/df) of the DSRR and the s-DSRR with a planar YIG film load. The DSRR has four pronounced photon modes, at 1.81, 2.77, 3.83, 5.79 GHz. The spiral resonator introduces additional modes at 1.48, 3.58, 5.42 GHz. To quantify and compare the MW photon-magnon coupling, the coupling strength, g , is typically used, which is directly obtainable from the experimentally (or numerically) acquired transmission spectra characterized by an anti-crossing gap⁸⁻¹⁴.

The coupling of all four DSRR modes to the YIG planar film were rather insignificant. For example, Fig. 2(b) shows the $[f, H]$ dispersion near a DSRR photon mode around 3.83 GHz. Only intermediate coupling strength is evident without the observation of a strong anti-crossing feature. However, another adjacent mode at 3.58 GHz that was caused by the spiral resonator exhibits a strong coupling with the YIG film, with a pronounced anti-crossing feature, Fig. 2(c). The coupling strength is estimated as $g/2\pi = 92$ MHz.

The same effect is also observed for using the YIG spheres. Likewise, Fig. 2(d) compares the DSRR and s-DSRR spectra with a YIG sphere load. Additional spi-

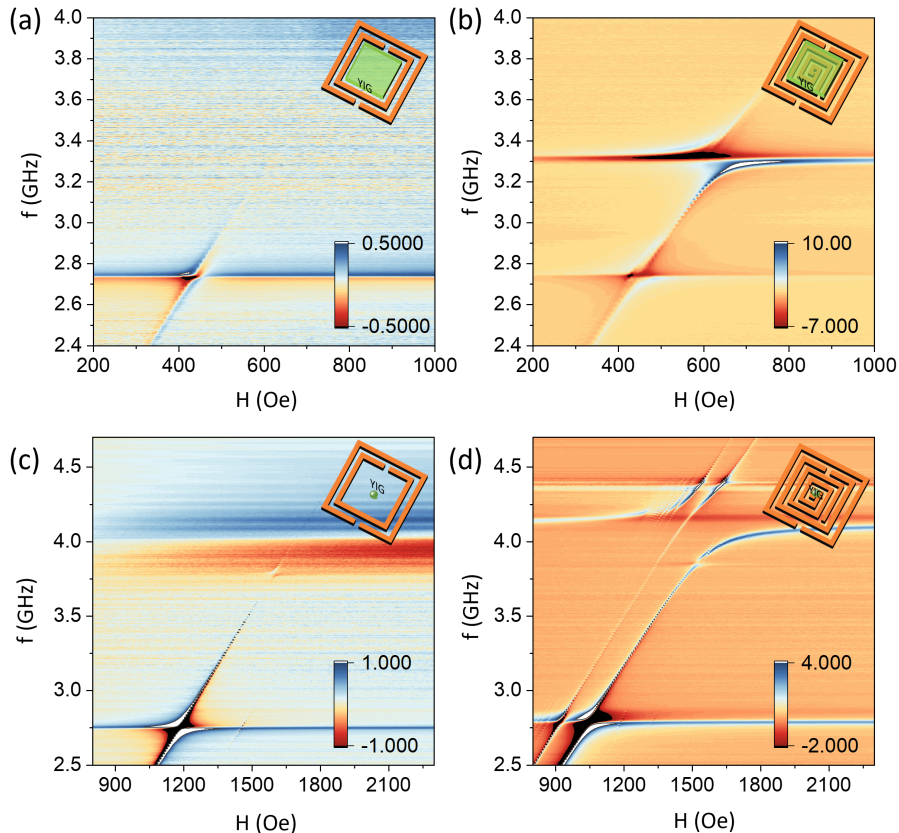


FIG. 3. Results for the edge-coupled (capacitive) resonator: 2D contour plot of the $[f, H]$ -dispersion showing the photon-magnon coupling. For YIG film: (a) with the DSRR resonator (trivial coupling), and (b) with the s-DSRR photon mode at 3.31 GHz. For YIG sphere: (c) with the DSRR photon mode (trivial coupling), and (d) with the s-DSRR photon mode at 4.16 GHz.

ral resonator modes (at 1.64, 1.93, 4.16, 5.76 GHz) beyond the DSRR modes (at 1.82, 2.78, 3.85, 5.82 GHz) can be observed. The YIG sphere generally couples stronger than the planar YIG film, for example, as shown in Fig. 2(e), where a nontrivial anti-crossing feature corresponds to $g/2\pi = 25$ MHz is observed. However, when looking at the nearby spiral resonator mode at 4.16 GHz, the coupling strength increased by more than tenfold, as shown in Fig. 2(f), with a $g/2\pi = 265$ MHz. Notably, the previous anticrossing feature at around 3.85 GHz due to coupling to the DSRR mode is still seen, whose coupling strength remains similar in magnitude to the case in Fig. 2(e).

Similar observation was also found for the other edge-coupled resonator, see Fig. 3. Such a configuration aims to increase the Q-factor via an enhanced capacitive coupling, but at a cost of additional microwave loss. Indeed, As shown in Fig. 3(a) and (c), the coupling using the generic DSRR photon mode at ~ 2.75 GHz is weak for both planar and spherical YIG loading. However, strong coupling emerges with the additional spiral structure at the spiral resonator modes, and a coupling strength of $g/2\pi = 105$ and 260 MHz were found for the YIG film,

Fig. 3(b), and sphere, Fig. 3(d), respectively.

By using the YIG sphere whose size is considerably smaller (diameter ~ 1.0 mm) than the dimension of the meta-resonator (9×9 mm² with metal/gap width ~ 0.5 mm), we can also study the spatial properties of the photon-magnon coupling at different locations of interest. Figure 4 summarizes the photon-magnon coupling with the spiral resonator mode at 4.16 GHz by attaching the YIG sphere at representative locations. Overall, the coupling strength reduces as the YIG sphere is moved away from the center of the spiral resonator. Following the strongest coupling at the center (Fig. 4(a)), slightly reduced coupling is observed when the YIG is placed off the center, at the inner spiral arm, see Fig. 4(b). The coupling rapidly decreases when the sample is further off-centered, for example, at the outer spiral arm, see Fig. 4(c), when the sphere is placed at the tail-end of the spiral and facing against the corner of the inner-SRR loop. On the other hand, by the above movement, the photon-magnon coupling with the DSRR mode at 3.85 GHz becomes progressively stronger, due to the closer proximity to the DSRR metallic loop that features a dominant inductive coupling, although the cou-

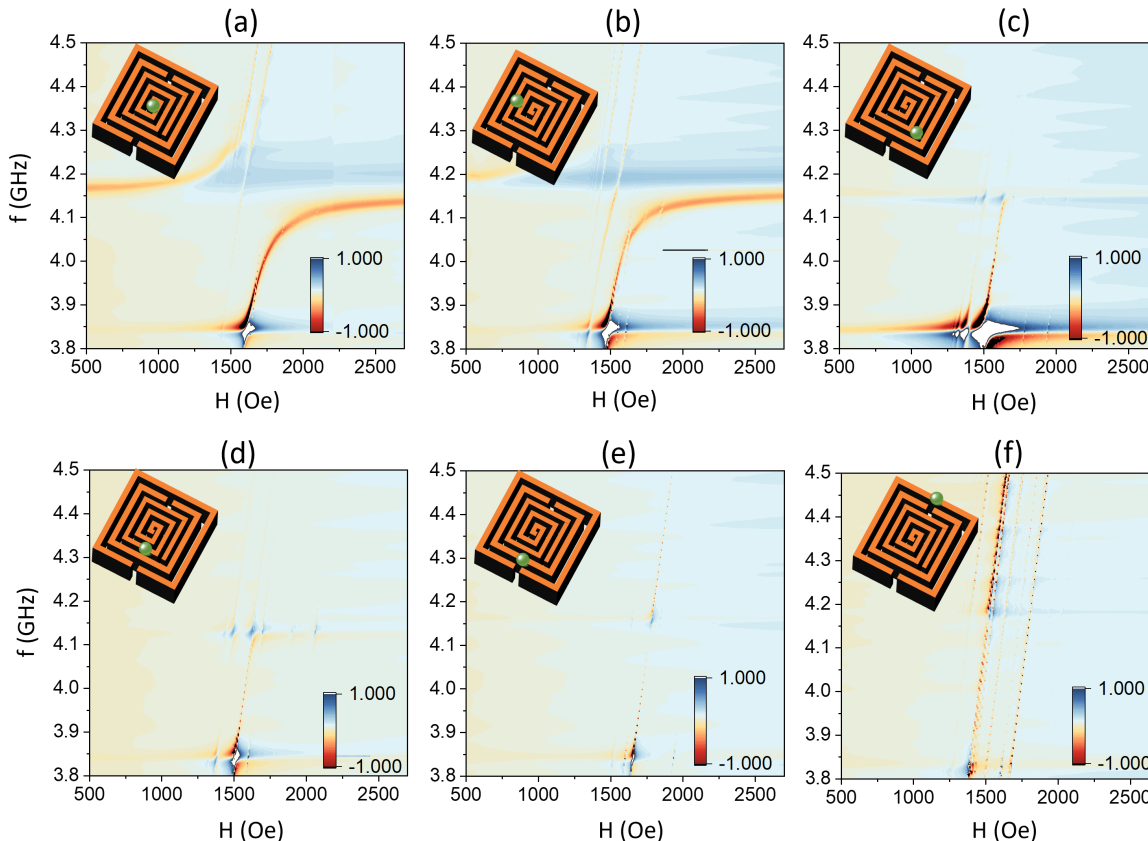


FIG. 4. 2D contour plot of the $[f, H]$ -dispersion showing the photon-magnon coupling between the YIG sphere and the s-DSRR photon modes at different representative locations: (a) center of spiral, (b) inner arm of spiral, (c) tail of spiral, against DSRR inner corner, (d) inner arm of DSRR, (e) outer arm of DSRR, away from stripline, and (f) outer arm of DSRR, close to stripline.

pling strength is still one order of magnitude smaller than spiral resonator mode. Last but not least, the photon-magnon coupling with both modes (s-DSRR: 4.16 GHz and DSRR: 3.85 GHz) is weak at the DSRR arm locations, for example, at the inner arm, Fig. 4(d), and at the outer arm, whether (the YIG sphere) is away, Fig. 4(e), or near, Fig. 4(f), the transmission line.

Finally, similar conclusion can be drawn from the other higher spiral resonator mode, at 5.42 and 5.76 GHz for YIG film and sphere loads, respectively, in Fig. 2(a) and (d). Enhanced photon-magnon coupling with notable anti-crossing gaps were found at the s-DSRR modes, as compared to the generic DSRR modes.

III. SIMULATION AND MODELING

To gain an in-depth understanding of the enhanced coupling, we performed simulation and modeling of the YIG-loaded DSRR and s-DSRR using the High Frequency Structure Simulator (HFSS) from ANSYS. The two-port microstrip line structure is used to excite the meta-resonators. Both the planar YIG and the spherical YIG are investigated, with the dimensions of the

YIG components given in section II B. Specifically, in HFSS, the permeability of the YIG component is modeled with the Polder's tensor⁴³ with the following material parameters: $M_s = 1750$ G, $\Delta H = 5$ Oe and Landé g -factor of 2. A uniform magnetic biasing field $H_0 = 0$ Oe is applied horizontally. The dielectric permittivity and the loss tangent of the YIG components are $\epsilon_r = 14$ and $\tan \delta = 0.0001$ respectively. The GGG substrate has the permittivity of $\epsilon_r = 11.99$ and the loss tangent $\tan \delta = 0.0052$. In both the planar and the spherical YIG cases, the s-DSRR is found to generate more resonant modes and significant frequency shift due to strong coupling.

To elucidate the nature of the extra resonances, we here take the planar YIG as an example and investigate the EM field distribution. As shown in Figure 5, three extra sharp resonances are observed in the s-DSRR case shown in solid lines, in contrast to the DSRR case in dashed lines. This agrees reasonably close with the measurement result in Figure 2 (a). Comparing the two sets of data in Figure 5, it is evidenced that the extra resonances noticed in the s-DSRR structure are created due to the spiral structure. As a further investigation, an eigenmode simulation of the s-DSRR resonator is con-

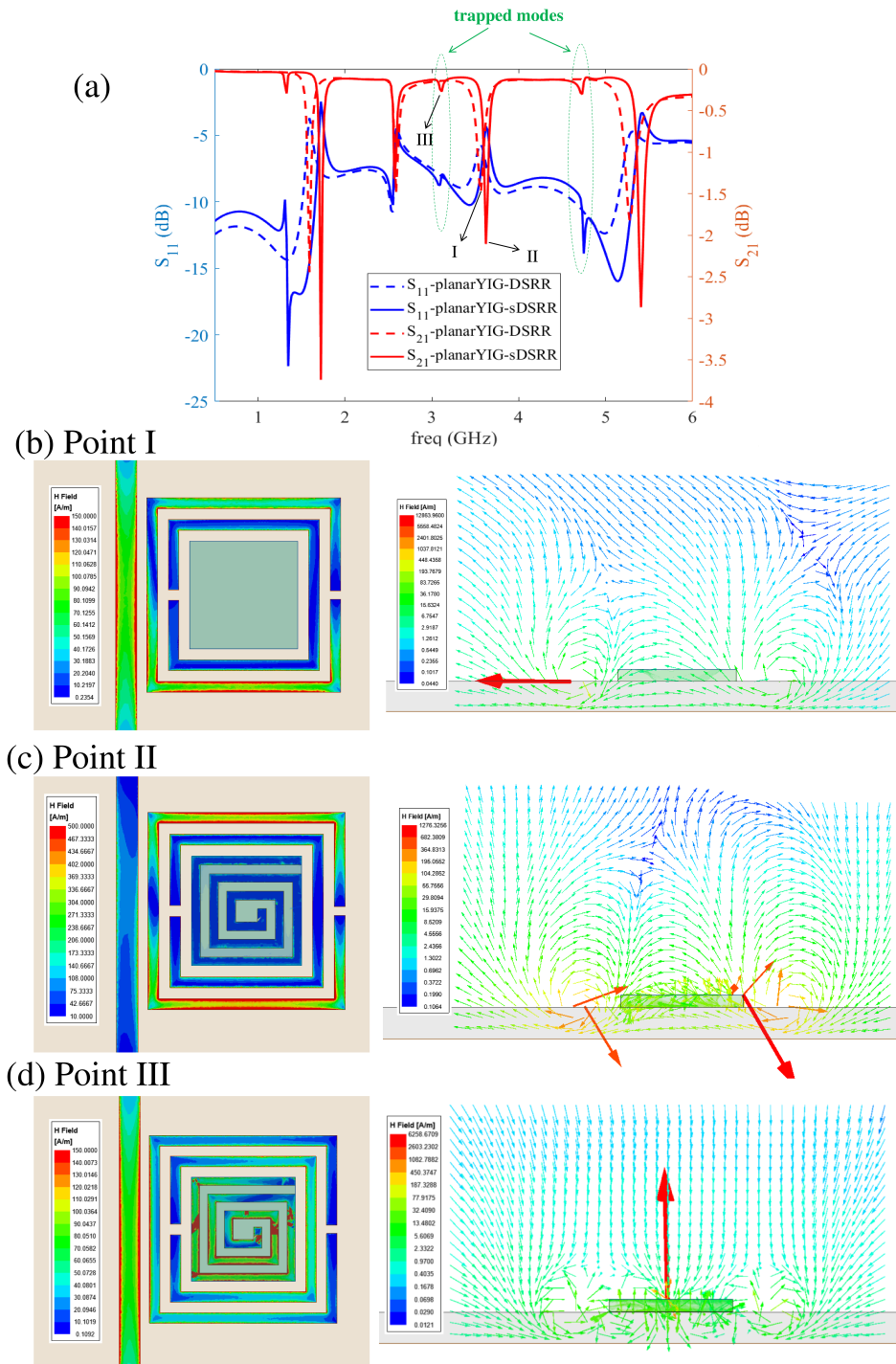


FIG. 5. (a) the simulated reflection (blue) and transmission (red) spectrum of the planar YIG loaded DSRR (dashed lines) and s-DSRR (solid lines) configurations; and the magnetic field distribution on the resonator and in the near field region for (b) point I (regular resonance point for DSRR at 3.564 GHz), (c) point II (regular resonance for s-DSRR at 3.620 GHz) and (d) point III (trapped mode for s-DSRR at 3.11 GHz).

ducted in Ansys HFSS. Similar resonances as reported in Figure 5(a) are observed in the eigenmode simulation. In addition, Fig. 6(a) and (d) show the surface current of the two modes at 3.62 GHz and 3.11 GHz respectively. While the resonance at 3.62 GHz is dominated by the

split-ring structure with primarily in-phase currents, the resonance at 3.11 GHz has dominant currents distributed over the spiral region with primarily anti-phase currents on all neighboring conductors. The anti-phase currents result in very weak coupling to radiation in free space, a

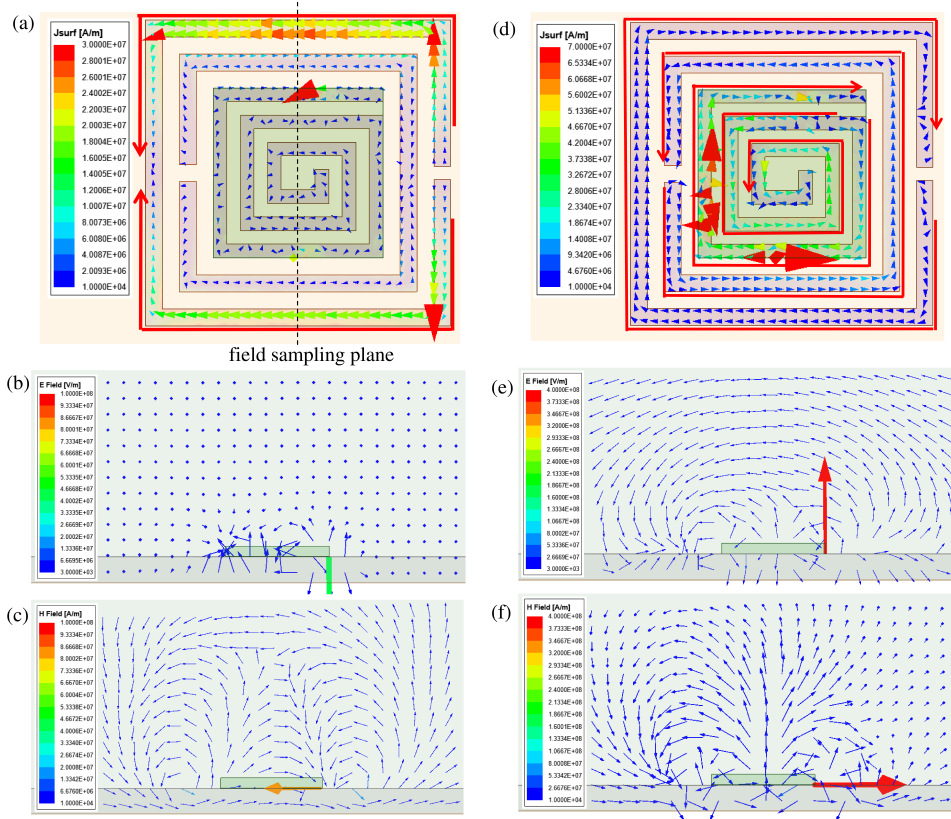


FIG. 6. The eigenmode surface current (a), eigen E field (b) and eigen H field (c) for the resonance at 3.62 GHz on s-DSRR; the eigenmode surface current (d), eigen E field (e) and eigen H field (f) of the spiral-induced trapped mode for s-DSRR at 3.11 GHz. Unit “stored energy” in each mode is used for normalization.

key feature of the trapped modes⁴⁴.

Next, we compare the simulated magnetic field distribution for the DSRR and s-DSRR with the planar YIG load. As an example, we focus on the spiral resonator modes with pronounced photon-magnon coupling, at 3.58 GHz in measurement (3.11 GHz in simulation) for the planar YIG. Figure 5(b) and (c) plot the dynamic magnetic fields on the metallic structure and in dielectric near field region of the regular (bright) modes, for the YIG-film-loaded DSRR and s-DSRR, respectively. For the DSRR, the strongest magnetic fields reside around the metallic arms of the split-structures. The magnetic fields inside the central dielectric area are overall weak, and are primarily polarized in the resonator plane. For the s-DSRR, on the other hand, the magnetic fields are significantly enhanced inside the central dielectric region due to the densely confined surface currents on and near the spiral metallic arms. The vector fields are strongly polarized perpendicular to the plane, which enhances the applied excitation along both the horizontal and vertical plane of the meta-resonator. As a validation check, the eigen E and H fields for the resonances at 3.62 GHz and 3.11 GHz are also provided in Figure 6(b)-(c) and (e)-(f) respectively. Similar magnetic field enhancement is observed for the trapped mode at 3.11 GHz.

In addition, Figure 5(d) plots the field distribution for

the trapped mode at 3.11 GHz, which is unique to the s-DSRR. An even stronger field concentration at the spiral resonator region and near the surface of the dielectric can be evidenced. The inner spiral arms and the spiral center also show stronger fields than the outer spiral arms. This ‘radial-like decay’ is in agreement with the general features of such spiral resonators, due to the radial decay of the structural asymmetry as the spiral arms become longer^{36–38}. Such a characteristic is also consistent with the earlier position-dependent measurements in Fig. 4, where the photon-magnon coupling quickly weakens as the YIG sphere is gradually moved away from the spiral structure.

IV. ANALYSIS AND DISCUSSION

Phenomenologically, the value of coupling strength g is directly proportional to the form factor η of the magnetic sample by the magnetic component of the resonator’s EM field, h , that is perpendicular to the external bias field, H , and the coupling strength can be written²³:

$$g = \frac{\gamma}{2} \eta \sqrt{\frac{\mu_0 S \hbar \omega_p}{V_m}}, \quad (1)$$

where γ is the gyromagnetic ratio, S is the total spin number, whose value is proportional to the magnetic moment of the magnetic sample and the number of spins (N_s), \hbar is the reduced Plank constant, μ_0 is the vacuum permeability, and ω_p is the photon mode frequency. The spin concentration (n_s) then relates to the total spins of the sample and the magnetic sample volume, by $n_s = N_s/V_m$. When the form factor $\eta = 0$, none of the resonator's h -field is perpendicular to the external bias field, whilst when $\eta = 1$, all of the h -field is perpendicular to the sample.

Notably, the role of η has been traditionally overlooked, and an estimation of the relationship: $g \propto \sqrt{N_s}$ is often claimed, hinting further: $g \propto \sqrt{V_m}$. However, increasing the volume of the sample also changes the η , therefore affecting the coupling strength. Such an effect can be corrected by taking into account the geometrical configurations like the magnetic filling factor, ζ_m , of cavity field contained in the sample by $g = \omega_c \sqrt{\chi_{\text{eff}} \zeta_m}$, where χ_{eff} is an effective susceptibility determined by material properties and the overlap of the specific cavity and magnon modes¹⁵. Therefore, the magnetic filling factor becomes the relevant figure of merit in maximizing the coupling strength.

In our hybrid design, the DSRR component induces a negative magnetic susceptibility for applied transverse EM waves, and its combination with a spiral resonator improves the electric and magnetic polarization and therefore further enhances negative electric and magnetic susceptibility. The mode volume of such dark mode is constricted due to its near-field confinement, which enables a strong spatial overlapping between the photon and magnon modes. Thus, the magnetic field distribution across the spiral structure increases the magnetic coupling within the spiral loop area and therefore enhances the magnetic filling factor of the sample²³.

Theoretically, The interaction³ between the individual

photonic components of this system (either the spiral or the DSRR) and the YIG sample can be modeled by two coupled classical oscillators O_1 and O_2 . Their equations of motion can be written as⁴⁵:

$$\ddot{x}_1 + \omega_c^2 x_1 + 2\beta\omega_c \dot{x}_1 - gx_2 = fe^{-i\omega t} \quad (2)$$

$$\ddot{x}_2 + \omega_m^2 x_2 + 2\alpha\omega_c \dot{x}_2 - gx_1 = 0 \quad (3)$$

where O_1 represents the s-DSRR and is driven by a plunger with a constant frequency ω . O_1 is connected to the plunger by a spring with resonant frequency ω_c . The plunger represents the microwave transmission line and applies a driving force to the spring. β is the damping due to a viscous force, α is the Gilbert damping factor, and g is the coupling strength between the two oscillators. O_2 is connected to a fixed wall by another spring with resonant frequency ω_m . To explore the effect of the coupling strength g and by extension, the magnetic filling factor ζ_m , the dispersion of this system must be calculated. x_1 and x_2 can be expressed as plane waves (x_1, x_2) = $(A_1, A_2)e^{-i\omega t}$. Using this representation, Equations (2) and (3) can be written in matrix form as:

$$\begin{pmatrix} \omega^2 - \omega_p^2 + 2i\beta\omega_c\omega & g \\ g & \omega^2 - \omega_m^2 + 2i\alpha\omega_c\omega \end{pmatrix} \begin{pmatrix} A_1 \\ A_2 \end{pmatrix} = \begin{pmatrix} -f \\ 0 \end{pmatrix} \quad (4)$$

The dispersion can be found by calculating the poles of the determinant of the interaction matrix \mathbf{M} . Since the coupling between the photon and magnon modes is what is being investigated, the region near where $\omega_c = \omega_m$ is all that is relevant. In this region, the detuning $\Delta\omega \ll \omega_c + \omega_m$, so a rotating wave approximation can be made⁴⁶. This simplifies the determinant to a form that can be easily solved. The dispersion, incorporating the magnetic filling factor ζ_m ¹⁵ discussed earlier, simplifies to:

$$\omega_{\pm} = \frac{1}{2} \left[\omega_m - \omega_c + i\omega_c(\alpha - \beta) \pm \sqrt{(\omega_m - \omega_c + i\omega_c(\alpha - \beta))^2 + 4\omega_c^2 \chi_{\text{eff}} \zeta_m} \right] \quad (5)$$

To evaluate the effect of the magnetic filling factor on the dispersion, the difference between the two solutions of the dispersion at the resonance condition ($\omega_c = \omega_m$) must be calculated:

$$\omega_{\text{gap}} = (\omega_+ - \omega_-)|_{\omega_c=\omega_m} \quad (6)$$

$$\omega_{\text{gap}} = \omega_c \sqrt{4\chi_{\text{eff}} \zeta_m - (\alpha - \beta)^2} \quad (7)$$

Experimentally determined values of these constants show that $g^2 \gg \alpha - \beta$, so $\omega_{\text{gap}} = 2\omega_c \sqrt{\chi_{\text{eff}} \zeta_m}$. Since O_1 represents the s-DSRR, the microwave transmission S_{21} is proportional to A_1 . Therefore, solving Eq. 4

for A_1 allows us to construct the $|S_{21}|^2$ spectrum. In this system, ω_c is the mode determined by the structure of the resonator and has no magnetic field dependence. However, ω_m has a field dependence determined by the shape of the YIG sample. For the samples investigated above, the field dependences are represented by the Kittel equations for a planar magnetic film, $\omega_m = \gamma \sqrt{(H + H_A)(H + 4\pi M + H_A)}$, where M is the magnetization of the sample and γ is the gyromagnetic ratio, and H_A is the uniaxial anisotropy energy. Using Fig. 3(b) as an example, modeling the additional spiral component mode at 3.31 GHz with a YIG planar film with $\gamma = 28$ GHz/T, the normalized $|S_{21}|^2$ spec-

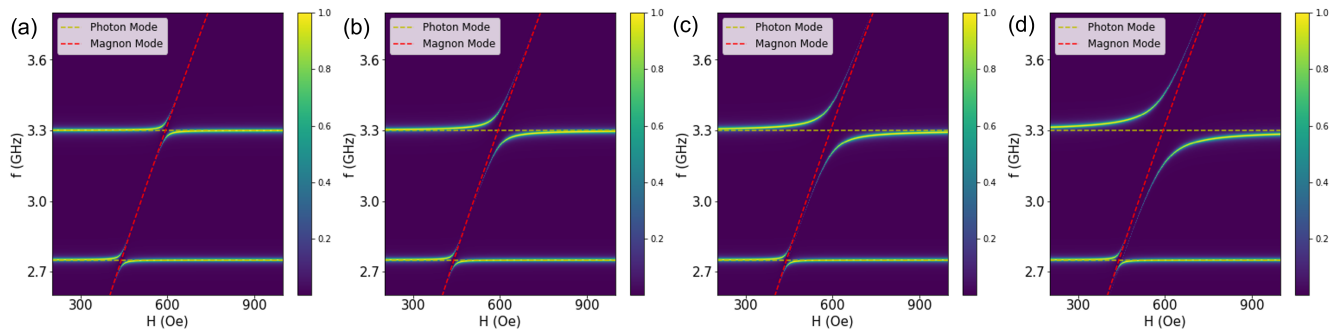


FIG. 7. Variation of the quantity τ (a) $\tau = 1$ (b) $\tau = 5$ (c) $\tau = 10$ (d) $\tau = 20$. The magnon mode for a planar YIG film was calculated by using the Kittel formula with a gyromagnetic ratio (γ) of 28 GHz/T (g -factor of 2) and a magnetization, M , of 0.175 T, and a uniaxial anisotropy energy, H_A , of 33.7 mT.

trum can be constructed. Since χ_{eff} is determined by material properties and its change is negligible with the addition of the spiral component, the increase in coupling strength g of the magnon to the spiral photon modes can be attributed to the associated increase in ζ_m ^{15,47}.

The basic interaction of a single photon mode with a single magnon mode can pave the way for analysis of more complicated interactions. According to experiments in Fig. 3(b), we found much stronger coupling of the YIG to the spiral mode at 3.3 GHz relative to the DSRR mode at 2.75 GHz. Since the spiral component alone would not couple strongly to the transmission line, the interaction can be modeled as an initial coupling between the DSRR mode and the magnon mode, followed by a second coupling between the spiral mode and the resultant cavity-magnon-polariton mode. Both interactions could be modeled simultaneously using a 3 x 3 interaction matrix, but this complicates the dispersion calculation immensely. The consecutive matrices method outlined above allows for the use of two separate 2 x 2 interaction matrices, and is also more physically consistent with this process. The first is identical to Eq.4, and the second replaces the magnon mode with the DSRR polariton mode dispersion. Since the coupling occurs in two steps, we can define a ζ_m^{DSRR} , which is the magnetic filling factor of just the YIG/DSRR system, and ζ_m^{spiral} , which is the filling factor of the combined YIG/DSRR/spiral system. Here we define the quantity τ , which is the ratio of ζ_m^{spiral} to ζ_m^{DSRR} .

The effect of changing τ on the $|S_{21}|^2$ spectrum is shown in Figure 7. At $\tau = 1$, the coupling strengths are identical. As τ increases, the coupling strength of the YIG to the spiral photon mode also increases, approaching the strength shown in Fig.3(b). This shows that the increase in coupling strength of the magnon to the additional spiral modes relative to the DSRR modes is a result of the increase in magnetic filling factor described in our coupled harmonic oscillator model.

In summary, we fabricated and characterized a combinatorial double-split-ring and spiral meta-resonator, and demonstrated its application for photon-magnon coupling in hybrid magnonics. Compared to the traditional

single split-ring, the use of a double-split-ring spectrally extends the bandwidth to a lower frequency region and spatially re-distribute the magnetic field towards the center of the resonator. In addition, the double-split-ring allows to further couple it to an additional metallic spiral resonator. The spiral resonator photon modes can be effectively excited owing to its strong coupling to the double-split-ring, which further gives rise to multi-resonance characteristics as well as an enhanced magnetic coupling (to magnetic samples) due to the increased filling factor and the formation of localized surface dark modes. Our results imply that the dark modes arising from meta-resonators hold a great promise towards strong photon-magnon coupling at room temperature, and have the potential to be miniaturized and integrated with auxiliary optical systems⁴⁸⁻⁵⁰.

ACKNOWLEDGMENT

The experimental work at UNC-CH was supported by the U.S. National Science Foundation (NSF) under Grant No. ECCS-2246254. The computational work at NCAT was supported by the U.S. NSF under Grant No. ECCS-2138741. Y. L. acknowledges support by the U.S. DOE, Office of Science, Basic Energy Sciences, Materials Sciences and Engineering Division under Contract No. DE-SC0022060. D.S. acknowledges support by the U.S. DOE, Office of Science, Basic Energy Sciences, under Contract No. DE-SC0020992.

- ¹G. Kurizki, P. Bertet, Y. Kubo, K. Mølmer, D. Petrosyan, P. Rabl, and J. Schmiedmayer, “Quantum technologies with hybrid systems”, PNAS **112**, 3866 (2015).
- ²D. Lachance-Quirion, Y. Tabuchi, A. Gloppe, K. Usami, and Y. Nakamura, “Hybrid quantum systems based on magnonics”, Applied Physics Express **12**, 070101 (2019).
- ³M. Harder and C. -M. Hu, “Cavity Spintronics: An Early Review of Recent Progress in the Study of Magnon-Photon Level Repulsion”, Solid State Physics, **70**, 47 - 121 (2018). R. Stamps and R. Camley (Ed.), Academic Press.
- ⁴D. D. Awschalom, C.H.R. Du, R. He, J. Heremans, A. Hoffmann, J. Hou, H. Kurebayashi, Y. Li, L. Liu, V. Novosad, J. Sklenar, S. Sullivan, D. Sun, H. Tang, V. Tyberkevych, C. Trevillian,

- A. W. Tsen, L. Weiss, W. Zhang, X. Zhang, L. Zhao, and Ch. W. Zollitsch, “Quantum Engineering With Hybrid Magnonics Systems and Materials”, *IEEE Trans. Quantum Engineering* **2**, 5500836 (2021).
- ⁵Y. Li, W. Zhang, V. Tyberkevych, W.-K. Kwok, A. Hoffmann, V. Novosad, “Hybrid magnonics: Physics, circuits, and applications for coherent information processing”, *J. Appl. Phys.* **128**, 130902 (2020).
- ⁶H.Y. Yuan, Yunshan Cao, Akashdeep Kamra, Rembert A. Duine, and Peng Yan, “Quantum magnonics: When magnon spintronics meets quantum information science”, *Physics Reports* **965**, 26, p1-74 (2022).
- ⁷A. A. Serga, A. V. Chumak, B. Hillebrands, “YIG magnonics”, *J. Phys. D.: Appl. Phys.* **43**, 264002 (2010).
- ⁸H. Huebl, C. W. Zollitsch, J. Lotze, F. Hocke, M. Greifenstein, A. Marx, R. Gross, and S. T. B. Goennenwein, “High Cooperativity in Coupled Microwave Resonator Ferrimagnetic Insulator Hybrids”, *Phys. Rev. Lett.* **111**, 127003 (2013).
- ⁹O. Soykal and M. E. Flatté, “Strong field interactions between a nanomagnet and a photonic cavity”, *Phys. Rev. Lett.* **104**, 077202 (2010).
- ¹⁰X.-F. Zhang, C.-L. Zou, L. Jiang, and H. X. Tang, “Cavity magnomechanics”, *Sci. Adv.* **2**, e1501286 (2016).
- ¹¹X. Zhang, C.-L. Zou, L. Jiang, and H. X. Tang, “Strongly Coupled Magnons and Cavity Microwave Photons”, *Phys. Rev. Lett.* **113**, 156401 (2014).
- ¹²Y. Tabuchi, S. Ishino, A. Noguchi, T. Ishikawa, R. Yamazaki, K. Usami, and Y. Nakamura, “Coherent coupling between a ferromagnetic magnon and a superconducting qubit”, *Science* **349**, 405 (2015).
- ¹³K. An, A. N. Litvinenko, R. Kohno, A. A. Fuad, V. V. Naletov, L. Vila, U. Ebels, G. de Loubens, H. Hurdequint, N. Beaulieu, J. Ben Youssef, N. Vukadinovic, G. E. W. Bauer, A. N. Slavin, V. S. Tiberkevich, and O. Klein, “Coherent long-range transfer of angular momentum between magnon Kittel modes by phonons”, *Phys. Rev. B* **101**, 060407(R) (2020).
- ¹⁴M. Fukami, D. R. Candido, D. D. Awschalom, and M. E. Flatté, “Opportunities for Long-Range Magnon-Mediated Entanglement of Spin Qubits via On- and Off-Resonant Coupling”, *PRX Quantum* **2**, 040314 (2021).
- ¹⁵Maxim Goryachev, Warrick G. Farr, Daniel L. Creedon, Yao-hui Fan, Mikhail Kostylev, and Michael E. Tobar, “High-Cooperativity Cavity QED with Magnons at Microwave Frequencies”, *Phys. Rev. Applied* **2**, 054002 (2014).
- ¹⁶B. Bhoi and S.-K. Kim, “Photon-magnon coupling: Historical perspective, status, and future directions”, *Solid State Physics*, **69**, 1 - 77 (2019). R. Stamps and H. Schultheiss (Ed.), Academic Press.
- ¹⁷Biswanath Bhoi, Bosung Kim, Junhoe Kim, Young-Jun Cho, and Sang-Koog Kim, “Robust magnon-photon coupling in a planar-geometry hybrid of inverted split-ring resonator and YIG film”, *NPG Sci Rep* **7**, 11930 (2017).
- ¹⁸Biswanath Bhoi, Bosung Kim, Hae-Chan Jeon, and Sang-Koog Kim, “Coupling-induced transparency and absorption in a magnon–multiphoton hybrid system”, *J. Appl. Phys.* **132**, 243901 (2022).
- ¹⁹Y. Li, T. Polakovic, Y.-L. Wang, J. Xu, S. Lendinez, Z. Zhang, J. Ding, T. Khaire, H. Saglam, R. Divan, J. Pearson, W. K. Kwok, Z. Xiao, V. Novosad, A. Hoffmann, and W. Zhang, “Strong Coupling between Magnons and Microwave Photons in On-Chip Ferromagnet-Superconductor Thin-Film Devices”, *Phys. Rev. Lett.* **123**, 107701 (2019).
- ²⁰J. T. Hou and L. Liu, “Strong coupling between microwave photons and nanomagnet magnons”, *Phys. Rev. Lett.* **123**, 107702 (2019).
- ²¹Yi Li, Timothy Draher, Andrew H. Comstock, Yuzan Xiong, Md Azimul Haque, Elham Easy, Jiang-Chao Qian, Tomas Polakovic, John E. Pearson, Ralu Divan, Jian-Min Zuo, Xian Zhang, Ulrich Welp, Wai-Kwong Kwok, Axel Hoffmann, Joseph M. Luther, Matthew C. Beard, Dali Sun, Wei Zhang, and Valentine Novosad, “Probing intrinsic magnon bandgap in a layered hybrid perovskite antiferromagnet by a superconducting resonator”, *Phys. Rev. Research* **5**, 043031 (2023).
- ²²Igor A. Golovchanskiy et al., “Ultrastrong photon-to-magnon coupling in multilayered heterostructures involving superconducting coherence via ferromagnetic layers”, *Sci. Adv.* **7**, eabe8638 (2021).
- ²³Graeme Flower, Maxim Goryachev, Jeremy Bourhill, and Michael E Tobar, “Experimental implementations of cavity-magnon systems: from ultra strong coupling to applications in precision measurement”, *New J. Phys.* **21**, 095004 (2019).
- ²⁴Biswanath Bhoi, Bosung Kim, Seung-Hun Jang, Junhoe Kim, Jaehak Yang, Young-Jun Cho, and Sang-Koog Kim, “Abnormal anticrossing effect in photon-magnon coupling”, *Phys. Rev. B* **99**, 134426 (2019).
- ²⁵S. Klingler, H. Maier-Flaig, R. Gross, C.-M. Hu, H. Huebl, S. T. B. Goennenwein, and M. Weiler, “Combined Brillouin light scattering and microwave absorption study of magnon-photon coupling in a split-ring resonator/YIG film system”, *Appl. Phys. Lett.* **109**, 072402 (2016).
- ²⁶Yongzhang Shi, Dongshan Zhang, Changjun Jiang, and Guozhi Chai, “Control of photon-magnon coupling with a nonuniform microwave magnetic field”, *J. Phys. D: Appl. Phys.* **52**, 305003 (2019).
- ²⁷J. Inman, Y. Xiong, R. Bidthanapally, S. Louis, V. Tyberkevych, H. Qu, J. Sklenar, V. Novosad, Y. Li, X. Zhang, and W. Zhang, “Hybrid magnonics for short-wavelength spin waves facilitated by a magnetic heterostructure”, *Phys. Rev. Applied* **17**, 044034 (2022).
- ²⁸Aleksey Girich, Sergiy Nedukh, Sergey Polevoy, Kateryna Sova, Sergey Tarapov, and Arthur Vakula, “Enhancement of the microwave photon-magnon coupling strength for a planar fabricated resonator”, *NPG Sci. Rep.* **13**, 924 (2023).
- ²⁹Claire M. Watts, Xianliang Liu, Willie J. Padilla, “Metamaterial Electromagnetic Wave Absorbers”, *Adv. Mater.* **24**, OP98-OP120.
- ³⁰Francisco J. Garcia-Vidal, Antonio I. Fernández-Domínguez, Luis Martín-Moreno, Hao Chi Zhang, Wenxuan Tang, Ruwen Peng, and Tie Jun Cui, “Spoof surface plasmon photonics”, *Rev. Mod. Phys.* **94**, 025004 (2022).
- ³¹J. Wu, Y. Li, F. Ding, H. Cheng, Z. Shen and H. Yang, “High-Order Localized Spoof Surface Plasmons Resonator for High Sensitivity Sensing,” *IEEE Sensors Journal* **22**, 12861-12868 (2022).
- ³²Hou-Tong Chen, Willie J. Padilla, Joshua M. O. Zide, Arthur C. Gossard, Antoinette J. Taylor, and Richard D. Averitt, “Active terahertz metamaterial devices”, *Nature* **444**, 597–600 (2006).
- ³³D. R. Smith, W. J. Padilla, D. C. Vier, S. C. Nemat-Nasser, and S. Schultz, Composite Medium with Simultaneously Negative Permeability and Permittivity, *Phys. Rev. Lett.* **84**, 4184 (2000).
- ³⁴Hongcang Guo, Na Liu, Liwei Fu, Todd P. Meyrath, Thomas Zentgraf, Heinz Schweizer, and Harald Giessen, “Resonance hybridization in double split-ring resonator metamaterials”, *Optics Express* Vol. 15, Issue 19, pp. 12095-12101 (2007)
- ³⁵J. B. Pendry, A. J. Holden, D. J. Robbins and W. J. Stewart, “Magnetism from conductors and enhanced nonlinear phenomena”, *IEEE Transactions on Microwave Theory and Techniques* **47**, 2075-2084 (1999).
- ³⁶Air Mohammad Siddiky, Mohammad Rashed Iqbal Faruque, Sabirin Abdullah, Mohammad Tariqul Islam, Mayeen Uddin Khandaker, and K. S. Al-Mugren, “Dual square split ring enclosed spiral shaped hybrid metamaterial resonator with size miniaturisation for microwave wireless applications”, *NPG Sci. Rep.* **12**, 8028 (2022).
- ³⁷F. Bilotti, A. Toscano and L. Vegni, “Design of Spiral and Multiple Split-Ring Resonators for the Realization of Miniaturized Metamaterial Samples”, *IEEE Transactions on Antennas and Propagation* **55**, 2258-2267 (2007).
- ³⁸B. Lopes, T. Ferreira, and J. N. Matos, “Design Guidelines for Gap Coupled Spiral Microstrip Resonators in Chipless RFID

- Tags”, *IEEE Journal of Radio Frequency Identification*, **4**, 525-531 (2020).
- ³⁹Sergey Polevoy, Aleksey Girich, Sergey Tarapov, Arthur Vakula, Sergey Nedukh, and Kateryna Sova, “Influence of the Magnet Filling Factor by the Field of Planar Resonators on the Photon-Magnon Coupling Strength”, *IEEE Conference Proceeding, 2022 IEEE 2nd Ukrainian Microwave Week (UkrMW)*.
- ⁴⁰H. Pan, J. Qian, Z. Rao, C. -M. Hu, and Z. H. An, “Spin pumping of magnons coherently coupled to a cavity dark mode”, *Phys. Rev. Appl.* **19**, 014075 (2023).
- ⁴¹V. A. Fedotov, M. Rose, S. L. Prosvirnin, N. Papasimakis, and N. I. Zheludev, “Sharp trapped-mode resonances in planar metamaterials with a broken structural symmetry”, *Phys. Rev. Lett.* **99**, 147401 (2007).
- ⁴²K. Masrakin, S.Z. Ibrahim, H.A. Rahim, S.N. Azemi, P.J. Soh, S. Tantivivat, “Microstrip Sensor Based on Ring Resonator Coupled with Double Square Split Ring Resonator for Solid Material Permittivity Characterization”, *Micromachines* **14**, 790 (2023).
- ⁴³D. Polder, “On the theory of ferromagnetic resonance”, *Physica*, **15**, 1, 253-255, (1949).
- ⁴⁴Fedotov, V.A., Rose, M., Prosvirnin, S.L., Papasimakis, N. and Zheludev, N.I., “Sharp trapped-mode resonances in planar metamaterials with a broken structural symmetry”, *Phys. Rev. Lett.* **99**(14), 147401, (2007).
- ⁴⁵Z. J. Tay, W. T. Soh, and C. K. Ong, “Observation of electromagnetically induced transparency and absorption in Yttrium Iron Garnet loaded split ring resonator”, *J. Magn. Magn. Mater.* **451**, 235–242 (2018).
- ⁴⁶Ying Wu and Xiaoxue Yang, “Strong-Coupling Theory of Periodically Driven Two-Level Systems”, *Phys. Rev. Lett.* **98**, 013601 (2007).
- ⁴⁷J. Bourhill, N. Kostylev, M. Goryachev, D. L. Creedon, and M. E. Tobar, “Ultrahigh cooperativity interactions between magnons and resonant photons in a YIG sphere”, *Phys. Rev. B*, **93**, 144420 (2016).
- ⁴⁸Mojtaba T Kaffash, Dinesh Wagle, Anish Rai, Thomas Meyer, John Q Xiao, and M Benjamin Jungfleisch, “Direct probing of strong magnon–photon coupling in a planar geometry”, *Quantum Sci. Technol.* **8** 01LT02 (2023).
- ⁴⁹Y. Xiong, J. Inman, Z. Li, K. Xie, R. Bidthanapally, J. Sklenar, P. Li, S. Louis, V. Tyberkevych, H. Qu, Z. Xiao, W. K. Kwok, V. Novosad, Y. Li, F. Ma, and W. Zhang, “Tunable magnetically induced transparency spectra in magnon-magnon coupled Y3Fe5O12/permalloy bilayers”, *Phys. Rev. Appl.* **17**, 044010 (2022).
- ⁵⁰D. A. Bozhko, A. J. E. Kreil, H. Y. Musiienko-Shmarova, et al. “Bogoliubov waves and distant transport of magnon condensate at room temperature”, *Nat Commun* **10**, 2460 (2019).